JOURNAL OF MATERIALS SCIENCE 32 (1997) 1799–1807

Strength and toughness of sintered plus forged T1 high speed steel

M. A. GOMES*, C. S. WRIGHT, A. S. WRONSKI
Engineering Materials Group, Department of Mechanical and Manufacturing Engineering, University of Bradford, Bradford, UK

The stresses for macroscopic plastic flow and critical stages of fracture, fracture toughness and hardness of sintered plus forged T1 high speed steel were determined. The results are compared to similar data for sintered, sintered to closed porosity plus hot isostatically pressed and electroflux refined (EFR) alloys of comparable composition. EFR meltstock, with addition of 0.6 wt% Mo, was water-atomized in a 200 kg unit which incorporated ceramic filters and an argon shroud to ensure maximum cleanliness. The powder was sieved, $<125\ \mu m$, vacuum annealed, blended, isostatically compacted and vacuum sintered and hot forged to produce a 300 kg billet. Mechanical properties were determined in four-point bending of heat-treated beam specimens. Most samples showed evidence of macroscopic plastic flow, up to $\sim 1\%$, beyond a stress of ~ 1.8 GPa, σ_Y. Using surface replica microscopy, crack nucleation was detected at stresses σ_N, between 0.5 and 0.9 σ_Y, and subcritical short crack growth, at stresses generally larger than σ_Y. Fracture, from crack nuclei associated (only) with fractured M_6C carbides, took place at stresses, σ_F, in the range 1.4 to 3.0 GPa Macroscopic fracture toughness, K_{IC}, was in the range 17–24 MPa $m^{1/2}$ and, like σ_N and σ_F, appeared to depend sensitively on the tempering temperature. The most attractive combination of properties, for the overtempered, 580 °C, structure at $HV_{50} \sim 750$ appears to be: $\sigma_Y \approx 1.9$ GPa, $\sigma_F \approx 2.8$ GPa, $K_{IC} \approx 23$ MPa $m^{1/2}$. These values are comparable to those for EFR aerospace quality T1 high speed steel.

1. Introduction

T1 high speed steel (HSS) also known as 18–4–1, i.e. 18W–4Cr–1V–0.8C steel, is one of the approved alloys for aerogas turbine bearings. These are subject to Hertzian contact stresses in excess of 2 GPa at rotational speeds reaching 25 000 r.p.m. The performance of HSS bearing materials has been improved radically in the last two decades through the use of superior melting and refining techniques resulting in significant improvements in alloy cleanliness. These techniques have little influence on the problem of anisotropy of the microstructure: carbide clusters and stringers in the direction of hot-working. This problem, though, can be overcome through the use of powder metallury (PM) techniques which result in more homogeneous, and finer, if so-desired, microstructures. Elimination of carbide stringers and clusters may lead to improvements in bearing performance and accordingly an European Union project was undertaken to investigate PM routes for manufacture of aeroengine bearings [1]. The baseline was wrought electroflux refined (EFR) material and we have published a preliminary comparison [1] of the deformation and fracture properties under monotonic loading of EFR, vacuum sintered (DS) and sintered/undersintered to closed porosity plus hot isostatically pressed (S + H) alloys of the same nominal composition.

Problems of residual porosity can be equally well solved by hot-working of the sintered material and the manufacturing route of vacuum sintering plus hot-forging was also investigated. This paper deals primarily with the mechanical properties of chemically similar material which has been processed on an industrial scale by sintering and subsequent forging, S + F. In our former and current investigations mechanical properties of heat-treated T1 HSS were investigated in four-point bending of smooth and notched and precracked, K_{1C}, specimens. An important feature of the results already reported is the detection, by surface replica microscopy, in specimens whose loading was interrupted before failure, of crack nucleation and subsequent "monotonic subcritical crack growth", at stresses below those for yield or fracture. The similarity of this phenomenon (occurring in the absence of a stress–corrosive environment) to that taking place in fatigue is to be emphasized. As failure of aeroengine bearings takes place by a rolling contact fatigue mechanism, these observations are of direct engineering relevance.

* Present address: Instituto de Soldadura e Qualidade, 2781 Oeiras Codex, Portugal.

In other HSSs, a water-atomized variant of ASP60 composition and T42 [2, 3], monotonic short crack growth has been the subject of earlier investigations; such a mechanism has also been observed and studied in ceramics [4–7] and composites [8, 9]. In many of these studies failures were reported at values of the (microscopic) stress intensity factor, K_a, below the (macroscopic) critical value, K_{IC}: termed the R-curve behaviour. A feature of this phenomenon is that the condition for catastrophic cracking can vary from specimen to specimen, or component to component. Study of the microstructural aspects of subcritical crack growth and catastrophic cracking in the microstructurally short crack regime is thus timely. Accordingly, the microstructural fracture mechanics of the S+F alloy will be reported and comparisons will be made with materials processed by different routes, and thus possessing somewhat differing microstructures.

2. Experimental details

The powder, for processing by sintering plus forging, was produced in a 200 kg capacity water atomization unit by Davy McKee, Sheffield, from an aerospace quality EFR bar supplied by Krupp. The melt filtration technique developed by Wright *et al.* [10] was employed and the tundish and atomization chamber were both protected by an argon shroud. To ensure sinterability [11] some 0.6 wt % Mo was added as ferromolybdenum to the melt and the carbon content was somewhat increased to balance for surface oxidation during powder processing. Powders from two runs (A and B, for which the chemical compositions are given in Table I) were sieved <125 μm, blended and annealed by Torvac in vacuo at 900 °C for 2 h. Care was taken to ensure all the powder received the required heat treatment under adequate vacuum: heating rate was adjusted to ensure vacuum did not deteriorate beyond 0.1 Pa, cooling rate was 50 °C h^{-1} to room temperature. The oxygen content of the as-atomized powder, $\sim$0.25 wt %, decreased to $\sim$0.10% as a result of the anneal. 300 kg of the industrially atomized and annealed powder, blended from the 2 runs, was cold isostatically pressed into a cylinder, sintered in vacuo at 1315 °C for 2 h and subsequently hot forged to full density at 1150 °C by Sintermetallwork Krebsoge into a billet 81 mm in diameter and some 6 m long.

Rectangular bend and fracture toughness specimens were cut with the prospective tensile axis parallel to the cylinder axis. The dimensions of the beams for four-point bending were 3.2 mm square with inner span of 15 mm and outer of 40 mm; K_{IC} samples were 2.8 mm × 10 mm (depth) with spans of 10 and 30 mm, respectively. The samples underwent a heat treatment in a vacuum/gas (nitrogen) quench furnace at the Loughborough University of Technology. Specimens were preheated at 850 °C for 10 min and then at 1050 °C also for 10 minutes prior to austenitization at 1240 °C for 6 min. Triple tempering, 1.5 h each at 525, 540 or 580 °C following quenching, resulted in HV_{50} values of 791, 860 and 753, respectively. Eventual chemical analysis is recorded in Table I.

The specimens were then ground and polished to final dimensions. In the case of bend specimens all the prospective tensile and some compressive faces were carefully lapped, finishing with 0.05 μm γ-alumina. The shape, though not the actual dimensions of the K_{IC} specimens, was according to BS5447 and a chevron notch was cut with a diamond impregnated disc blade 0.5 mm thick. The precrack was introduced by an impact technique, developed by Eriksson [12] and used successfully at Bradford [13–16]. It yields K_{IC} values comparable to those obtained by fatigue precracking in cemented carbides and high speed steels [17].

The beam specimens were tested on a Hedeby machine at a rate of 0.1 mm min^{-1}. To enable surface replicas of loaded specimens to be taken, a special jig [3] was used for the bend specimens. Load was measured by a BLH strain gauge cell and mid-span deflection by a LVDT. Outputs of these sensors were fed to an X–Y recorder. The surface replication technique used acetyl cellulose film 0.034 mm thick and 9% methanol in dichloromethane as the solvent. A few drops of the solvent were first placed on the polished surface to be replicated and the plastic film on top. After allowing the solvent to evaporate (2 min), the replica was stripped using soft cardboard with double-sided sticking tape. Prior to examination, mainly by optical microscopy, the replicas were sputter coated with gold for 4–6 min. The replicas were taken first on undeformed specimens and then several times during their loading, so that a record of pre-failure damage could be kept. To obtain replicas of compressive faces, the specimens were unloaded and taken out of the jig.

Most of the optical examinations were performed on a Reichart-Jung MeF3 microscope using the Nomarski interferometric technique. Sizes of prior austenite grains were determined after etching in 5% nital. Scanning electron microscopic examinations, especially fractographic analyses, were carried out on a Jeol instrument fitted with a Link X-ray microanalyser. Sizes, shapes and volume fractions of carbides were statistically analysed using the Joyce–Loebel Genias 125 quantitative image analyser.

TABLE I Chemical composition in wt % of the powder batches A and B and of the sintered plus forged T1 (compositions of DS and S+H variants were similar and EFR had 0.48 wt % Mo)

Material	C	S	P	O_2	Mo	Cr	W	V	Si	Mn	Fe
Powder A	0.96	0.003	0.019	0.24	0.60	3.98	17.55	1.97	0.3	0.19	Bal.
Powder B	0.99	0.008	0.023	0.30	0.61	4.14	17.66	1.07	0.4	0.1	Bal.
Product	0.79	0.001	0.022	0.005	0.56	4.09	17.51	1.10	0.25	0.20	Bal.

3. Results

3.1. Microstructures

The microstructures of the three S + F materials were similar with average grain sizes in the range 10–15 μm and volume fractions of M_6C carbides of ~17%. The sintered plus forged microstructure is illustrated together with those of sintered, sintered plus HIPed and conventional wrought T1 in Fig. 1. Some, generally rounded, MC carbides up to 20 μm in size were present, but <1% by volume and only in the wrought material, resulting from segregation during solidification. These were identified by energy dispersive spectroscopy (EDS), as usually in HSSs MC carbides are V rich, whereas M_6C carbides contain predominantly Fe and W. These are also generally smaller and large amounts of these, 1–2 μm in size, were evident. Their average size was 2.6 μm, with a maximum of ~25 μm. The circularity of the carbides was 0.91 on average, though it ranged from 0.1 to 1.0. The cleanliness of the alloy, resulting from the use of ceramic filters, was high (comparable to EFR stock) and inclusions were not detected in S + F T1 specimens; neither were pores. In spite of the forging (some 88% reduction in area), no banding of carbides was detected, in marked contrast to the EFR material in which stringers, some 20–40 μm apart, are a characteristic feature of the microstructure.

3.2. Bend tests

Most of the S + F specimens tested showed deviations from linearity on the load–deflection traces and the relevant load, P, was used to compute the Young's modulus, E, and the yield strength (stress at the linearity limit):

$$\sigma_Y = \frac{3P(o-i)}{2BW^2} \quad (1)$$

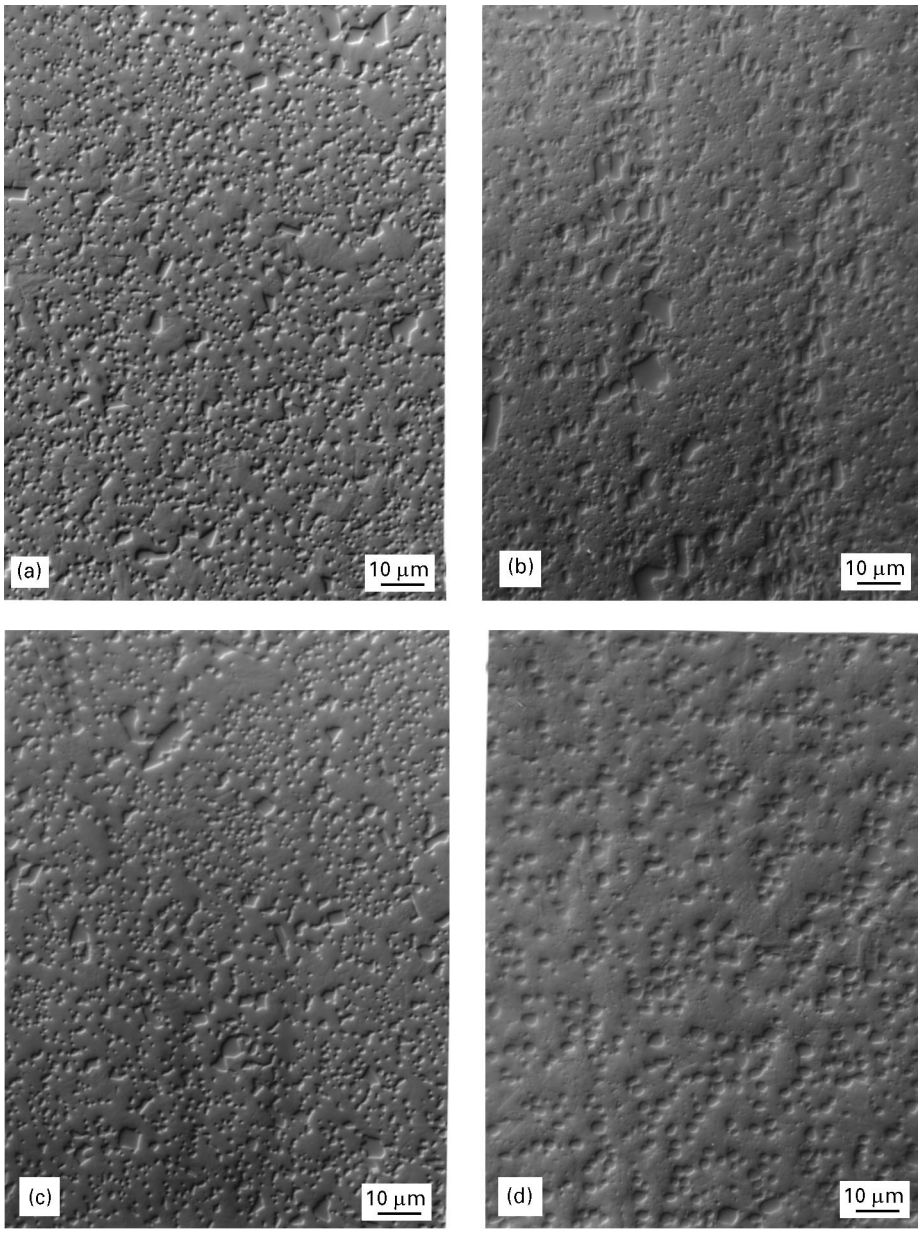

Figure 1 Microstructures of the four types of T1 HSS whose properties are being compared: (a) as-sintered (at 1310 °C), (b) wrought, (c) sintered plus HIPed and (d) sintered plus forged.

where o and i are the outer and inner spans, B, the specimen width and W, its depth. σ_Y values were evaluated to be near 1.8 GPa (Table II). By taking account of subsequent work-hardening, H, assuming it to be linear at a rate $H < E$, stresses at fracture, σ_F, were calculated [18]. It is to be noted that the σ_F values for specimens exhibiting limited plasticity are lower than those calculated using Equation 1, the "elastic" beam formula. In Table II, plastic strains to failure, ε_P, 0 to 0.97%, stresses for crack nucleation, σ_N, and subcritical crack growth, σ_G, macroscopic fracture toughness, K_{IC}, and, for the fracture strength values, Weibull moduli, m, are also recorded. It is to be noted that m at 6 and 7 for the lower tempering temperatures is low for high quality HSS, indicating that a simple analysis is probably inapplicable and that more than one type of failure initiation mechanism may operate; m of 19 for the 580 °C temper appears very satisfactory. For comparison, some data for EFR, DS and S+H materials [1, 3] of comparable cleanliness are also tabulated. These latter alloys were all austenitized at 1240 °C and triple tempered at 540 °C, i.e. they should be compared in terms of microstructure to S+F (540).

3.3. Fracture toughness

The precrack front in K_{IC} specimens was sometimes difficult to delineate in the fractured samples, hence these K_{1C} specimens were etched in 5% nital prior to testing. The crack depth, a, employed in Relation 2 was an average of five measurements spaced equally across the somewhat curved crack front. Only results from specimens satisfying the requirement $0.1W < a < 0.6W$, where W is the specimen depth, were used to evaluate K_Q from the formula:

$$K_Q = \frac{3P(o-i)a^{1/2}}{2BW^2}\left[1.99 - 2.47\left(\frac{a}{W}\right) + 12.97\left(\frac{a}{W}\right)^2 - 23.17\left(\frac{a}{W}\right)^3 + 24.80\left(\frac{a}{W}\right)^4\right] \quad (2)$$

where the symbols have the same meaning as in Relation 1. The K_Q values can be considered as valid K_{IC}, and were so recorded in Table II, as the requirement, $W > 2.5\ (K_Q/\sigma_Y)^2$, which approximates to 250–300 μm, is easily satisfied. The typical, for HSSs, decrease of toughness with increasing hardness from $\sim 23\ \mathrm{MPa\,m^{1/2}}$ at $750\ \mathrm{HV_{50}}$ to $\sim 16\ \mathrm{MPa\,m^{1/2}}$ at $850\ \mathrm{HV_{50}}$ (comparable to EFR data) is to be noted.

3.4. Crack nucleation

The prevalent sites of crack nucleation in S+F T1 HSS were M_6C carbides. Fractured M_6C carbides, typically up to 25 μm in size, were generally detected at stresses between 0.8 and 1.6 GPa, σ_N, i.e. between 0.5 and 0.9 σ_Y (e.g. Figs 2, 3a and b). The stress levels

TABLE II Summary of mechanical properties of wrought (EFR), sintered (DS), sintered plus HIPed (S+H) and sintered plus forged (S+F) T1 HSS (525, 540 and 580 for S+F refer to tempering temperatures in °C)

		Batch					
		EFR	DS	S+H	S+F		
					525	540	580
Number of specimens		15	9	9	12	15	14
E (GPa)	min			222	213	218	230
	mean			225	230	239	241
	max			227	243	256	250
σ_Y (GPa)	min		2.08	2.18	1.60	1.78	1.68
	mean		2.11	2.22	1.69	1.95	1.86
	max		2.14	2.25	1.78	2.15	2.04
σ_N (GPa)	range		1.12[a] −1.86	1.29 −1.30	0.98 −1.10	0.81 − 1.06	1.49 −1.59
σ_G (GPa)	range		1.68 −2.12	2.25 − 2.29	n.d.[b]	2.05 − 2.13	2.53 −2.68
σ_F (GPa)	min	1.95	1.70	2.00	1.35	2.02	2.66
	mean	2.70	2.20	2.52	1.80	2.38	2.83
	max	3.38	2.42	3.33	2.37	2.94	3.01
ε_P (%)	min		0	0.06	0	0.10	0.52
	mean			0.13	0.20	0.42	0.79
	max			0.31	0.50	0.97	0.92
Weibull modulus, m				6 ± 1.5	6 ± 1.4	7 ± 1.2	19 ± 4.3
Number of specimens		13			5	5	5
K_{IC} ($\mathrm{MPa\,m^{1/2}}$)	min	15.6			16.8	14.6	22.3
	mean	17.3			17.5	15.6	23.2
	max	18.6			18.6	16.6	24.1

[a]From pore at < 0.85 GPa.
[b]Not detected.

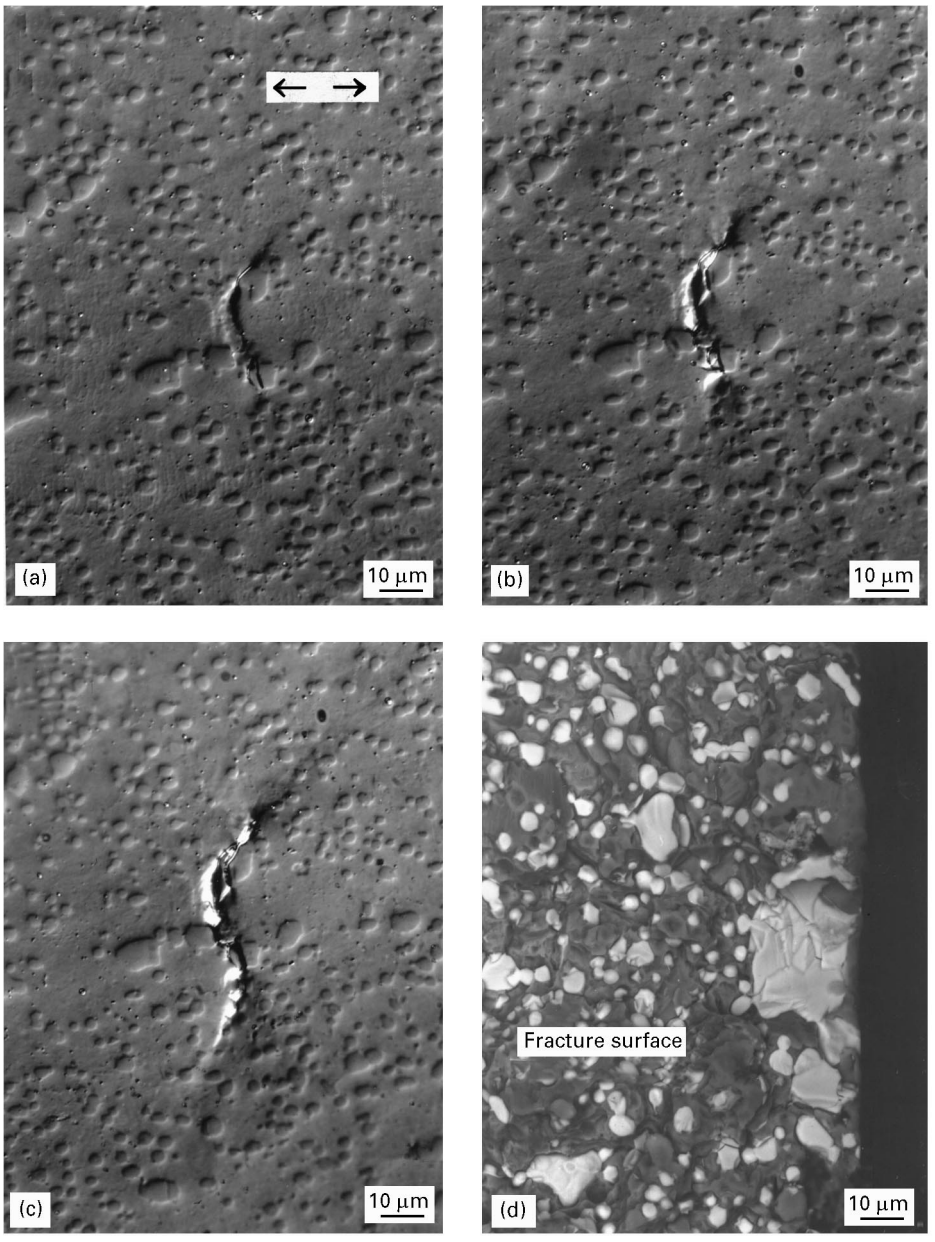

Figure 2 Details of the failure process in a sintered plus hot forged T1 specimen, tempered at 580 °C, which yielded at 1.84 GPa and fractured at 2.72 GPa. Tensile axis indicated by arrows. (a) Failure initiation in 2 separate carbides, $\sigma_N < 2.15$ GPa. Crack extension observed at (b) 2.27 GPa and further subcritical crack growth at (c) 2.37 GPa. (Note that this microcrack growth appears to follow prior austenite boundaries lying approximately transversely to the tensile axis.) (d) Scanning electron fractograph of the failure originating region containing the relevant carbides, showing their real subsurface sizes.

were the same in tension and compression (e.g. Fig. 3c). At higher stress levels, approximating to the yield stress, matrix cracking was subsequently detected in compression in S + F T1 (e.g. Fig. 3d). It should be noted that the stress levels for carbide cracking in S + F T1 are lower in the specimens tempered at 525 and 540 °C than for those at 580 °C: 1.5–1.6 GPa (0.8–0.9 σ_Y).

3.5. Subcritical crack growth

Growth and arrest of microcracks from the cracked carbides, as the applied stress was increased in steps of some 10% σ_F, e.g. Fig. 2, was detected in the majority of the specimens (though not those tempered at 525 °C). The stress values for this static subcritical crack growth (in the absence of a corrosive environment or dynamic loading), σ_G, were generally in excess of those for yielding; typically $1.05\sigma_Y < \sigma_G < 1.45\sigma_Y$ (Table II). Subcritical crack extension was dependent on details of the microstructure, and in particular, favoured paths were prior austenite grain boundaries. Lengths of the subcritical cracks measured on the tensile surfaces, $2c$, were up to 60 μm.

Cracks were assumed to be semi-elliptical, with (surface) major axis, $2c$, and semi-minor axis, a. Microscopic stress intensity factors, K_a, were calculated with a further assumption of semicircular geometry of microcracks, i.e. $c = a$ (crack depth). In the case of T1 (in contrast to other data on HSSs [3]) the critical values of K_a, calculated using the $2c$ value recorded at the last stress arrest and the stress of fracture, σ_F, approached the macroscopic value of K_{IC}, independently evaluated using long cracks. When, subsequent

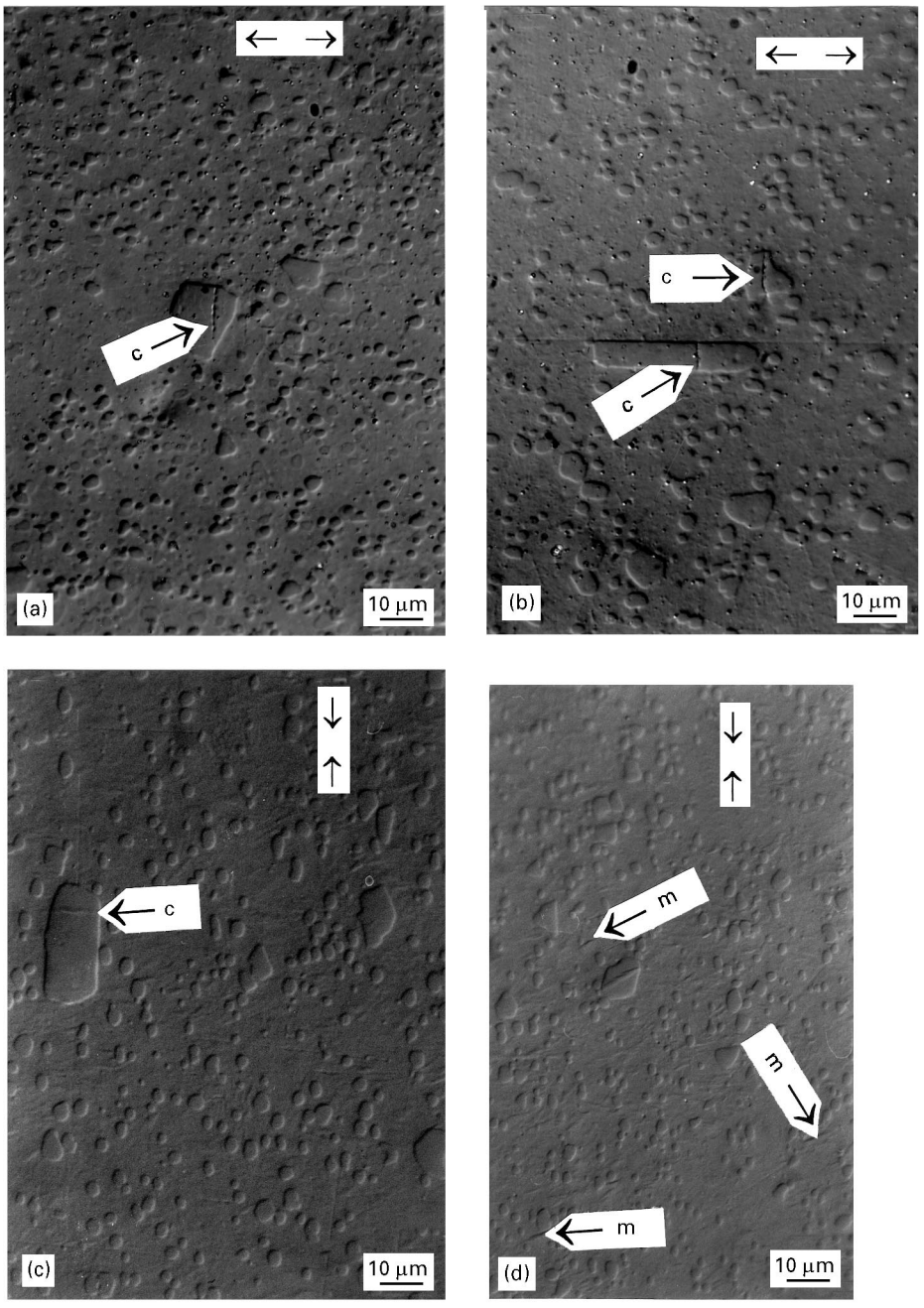

Figure 3 Non-propagating microcracks observed on the tensile and compressive faces of unfractured bend T1 HSS specimens (a) tension, $\sigma = 1.20$ GPa, (b) tension, $\sigma = 1.50$ GPa, (c) compression, $\sigma = 1.15$ GPa, and (d) compression, $\sigma = 1.96$ GPa (matrix cracking, m, at approximately the yield stress). Note the similar values of the compressive and tensile stresses and variability of microcrack orientations (including transversal) with respect to the compressive axis (c). Tensile and compressive axes indicated by arrows.

to specimen fracture, non-propagating cracks on the tensile surfaces were examined, they were found to be shallow: $a < 6\ \mu m < c$.

3.6. Fractography

In contrast to these dormant microcracks, failure initiation took place from approximately semicircular sites (e.g. Fig. 2d), sometimes associated with the characteristic "river markings". It is to be noted that no failures associated with porosity or inclusions [1, 3] were detected, attesting to high microstructural quality and cleanliness of vacuum-sintered water-atomized powder. The critical crack depths, a, were up to $\sim 20\ \mu m$, in reasonable accord with maximum $2c$ values, up to 60 μm, recorded by replica surface microscopy.

4. Discussion

The yield and fracture strengths of electroflux refined and water-atomized, vacuum-sintered and hot-forged aerospace quality T1 high speed steels are comparable. For the properties of EFR material reference can be made not only to Table II, but also to our previous report [1], and to the paper by Rescalvo and Averbach [19], who tested tensile and standard fracture toughness specimens. The improvement in fracture strength due to the hot-forging operation is to be noted, except for the case of the 525 °C temper. The

other S+F and S+H specimens have strengths near those of EFR samples. This is postulated to be related to closure of (the few) residual pores [1, 3], still present after direct sintering (DS). The other important factor, distinguishing this vacuum sintered material from conventional PM HSSs, is the application of the melt filtration technique [10]. Its effectiveness is demonstrated by the failure to detect (in this limited investigation) of failure initiation from inclusions. These defects have sometimes been shown to be responsible for failure initiation in conventional wrought materials and those HSSs sintered from conventionally water-atomized powders [1, 3].

In one respect the S+F structure is considered superior to that of the EFR material: absence of carbide stringers. These play a role in crack nucleation and growth [1, 3], as illustrated in the replica sequence and fractograph of Fig. 1 of [1], and therefore are to be avoided in the quest for optimization of resistance to fracture by monotonic and fatigue (especially rolling contact) loading.

Attention should be drawn to the significant improvement, 30–50%, in the fracture toughness of S+F material caused by increasing the tempering temperature to 580 from 540 or 525 °C. This has been accomplished at the expense of a drop in hardness, to 751 from 860 and 791 HV_{50}, but is considered worthwhile in the context of bearing applications, as an overtemper is recommended [19, 20]. The underlying microstructural reasons, as they are associated with detailed changes occurring during secondary hardening, are unknown, although transmission electron microscopic studies of secondary hardening have been attempted [21, 22]. In a number of HSSs [22] it has been shown that secondary hardening is due to the precipitation of M_2C and MC carbides. Overtempering was associated with coarsening of these precipitate dispersions. Moreover, correlation of change in properties with specific microstructural modifications is not yet possible due to the extreme complexity of the tempered martensitic structure of high speed steels.

There are also aspects of the microstructure and properties of sintered and forged T1 which are worthy of comparison with material which has been manufactured by the gas atomization plus hot isostatic pressing route. Such a HSS, (pre 1994) ASP60, has been concurrently studied and reported on [2, 3]. Its microstructure is characterized by small, up to 6 μm, M_6C and MC carbides with a mean free path between them of only ~1.5 μm. Although some of the carbides were observed to debond from the matrix when ASP60 beam specimens were loaded to stresses in the range 1.25–1.60 GPa, "all" the failures identified in that study were associated with calcium-alumino silicates, which also debonded. These, in the absence of subcritical crack extension, acted as failure nuclei at higher stresses, generally >2 GPa and subsequent to macroscopic yielding [2, 3], i.e. comparable in magnitude to our 580 °C tempered S+F T1.

Cleanliness is a factor well-recognized by the producers of HIPed HSSs and papers at PM '94 [23, 24] report on the improvement in the processing technology and resultant mechanical properties. The very fine rounded microstructure of the carbides, consequent to processing below the solidus temperature (in contrast to liquid phase sintering of our DS material), is retained in the improved ASP alloys. The advantages of this fine microstructure regarding grindability are established; whether fine microstructure is desirable when the HSS is acting as a cutting tool remains to be verified. What has, however, been reported a number of times [2, 25, 26], is a consequence of this very fine microstructure on the (macroscopic) fracture toughness, K_{IC}. Values for ASP-type alloys, especially at lower hardness levels, are consistently lower than for vacuum-sintered counterparts. This has been associated [2, 26] with the small interparticle (carbide) spacing in these alloys, λ, ~1.5 μm. Accordingly the size of the plastic zone, r_P ~2 μm, ahead of the long crack necessarily present in K_{IC} specimens, is comparable to λ, and therefore the plastic zone is likely to contain a brittle carbide, leading to low K_{IC}. In smooth specimens the observed critical defect sizes in HSSs are typically 2–100 μm, and thus it is not evident that resistance to the propagation of much longer cracks is an important property for high speed steels (as cutting or wear materials). It should be noted, however, that the K_{IC} values for S+F (580) at ~23 MPa $m^{1/2}$ are approximately double those of heat-treated ASP60 of comparable hardness. Consistent with the earlier analysis, the relatively high K_{IC} value for S+F material can be associated with the size of the plastic zone, r_P, 5–11 μm, being in general no longer than the interparticle spacing, λ, 8–13 μm.

At $K_{IC} = 24$ MPa $m^{1/2}$, r_P is comparable to λ and therefore optimum particle size (for the given chemical composition) to maximize K_{IC} has been attained. It should, however, be added that, if crack initiation is associated only with carbides and crack growth difficult, decrease in precipitate size could still lead to higher fracture strengths. Let us consider crack propagation being the critical stage in fracture at a stress $\sigma_P = \sigma_F$. Assuming a surface crack of depth, a, and semicircular geometry, acting as a nucleus for catastrophic fracture, the strength, σ_F, for various values of a, σ_Y, K_{IC} can be evaluated from Irwin's formula [27]:

$$a = \frac{K_{IC}^2}{1.2\Pi\sigma^2}\left[2.467 - 0.212\left(\frac{\sigma_F}{\sigma_Y}\right)^2\right] \quad (3)$$

or:

$$\sigma_F = \left[\frac{1}{(1.53/K_{IC}^2) + (0.086/\sigma_Y^2)}\right]^{1/2} \quad (4)$$

assuming macroscopic fracture mechanics is applicable. This may well not be so for microstructurally short cracks, not only in fatigue, but also in monotonic loading in HSSs [2, 3].

Table III lists the fracture strengths, σ_F, calculated using Relation 4 for a yield strength of 1.8 GPa and a realistic range of K_{IC}: 12–24 MPa $m^{1/2}$ and crack depth (half diameter): 2–100 μm. The σ_F values above $\sigma_Y = 1.8$ GPa are on the left hand side of Table III. The correlation with macroscopic fracture mechanics is reasonable to the right, but not for $a < 10$ μm. This

TABLE III Computed stresses, σ_F (GPa), for propagation of surface semicircular cracks of depth, a, in material of $\sigma_Y = 1.8$ GPa and fracture toughnesses, K_{IC}

K_{IC} (MPa m$^{1/2}$)	a (μm)							
	2	5	10	15	25	30	50	100
12	4.6	3.5	2.7	2.3	1.9	1.7	1.3	1.0
15	5.0	4.1	3.3	2.8	2.3	2.1	1.7	1.2
18	5.3	4.5	3.7	3.2	2.6	2.4	2.0	1.4
21	5.5	4.8	4.0	3.6	3.0	2.8	2.2	1.6
24	5.6	5.0	4.3	3.9	3.3	3.1	2.5	1.9

is consistent with observations of failure at applied $K_a < K_{IC}$, R-curve behaviour, for the microstructurally short crack regime reported for HSSs [2, 3].

The point about $\sigma_F > \sigma_Y$ in the presence of cracks needs making for these relatively brittle materials. Macroscopic fracture toughness is a relevant material parameter for structural applications, not the end use of HSSs. It is encouraging to report consistent evidence of macroplasticity, approaching 1%, in fully heat-treated "sintered" (+forged) high speed steel, in accord with the results on EFR material. Similarly, in contrast to the DS batches, in EFR [1, 3] and S+W, little evidence of monotonic subcritical crack growth was detected. When it was, the stress level, σ_G, was generally above σ_Y (Table II), even in the microstructurally favourable situation of growth along prior austenite grain boundaries approximately transverse to the tensile axis between two crack nuclei (Fig. 2). Thus, it appears possible to process water-atomized HSS powder, in batches up to 400 kg, to produce uniform microstructures, free of pores and inclusions to the standard currently required for EFR material. Resultant fully heat-treated alloy exhibits macroscopic ductility, and although crack nucleation, associated with carbides, takes place below σ_Y, subcritical crack growth (governed by texture in a way similar to fatigue loading [28]) generally takes place only at $\sim$2.5 GPa, in material which yields generally below 2.0 GPa.

5. Conclusions

1. Macroscopic mechanical properties of powder metallurgy T1 high speed steel manufactured into a 300 kg billet (the processing involved melt filtration, powder sieving and hot forging of the sintered bar) are comparable to those of aerospace bearing-quality electroflux refined material.

2. Mechanical properties of our sintered and hot forged T1 have been found to be sensitively dependent on the secondary hardening heat treatment with the overtempered structure, triple 580 °C temper, possessing this attractive "combination" of mechanical properties:

(a) yield strength $\sigma_Y \approx 1.9$ GPa, fracture strength $\sigma_F \approx 2.8$ GPa,

(b) fracture toughness $K_{IC} \approx 23$ MPa m$^{1/2}$, and

(c) total $\varepsilon \approx 1.6\%$ and plastic $\varepsilon \approx 0.8\%$ at hardness $HV_{50} \approx 750$.

3. Stresses for crack nucleation, σ_N and monotonic subcritical crack growth, σ_G, were determined using surface replica microscopy on bend specimens whose loading was arrested several times before fracture. Generally the respective stresses were $0.5\,\sigma_Y < \sigma_N < 0.9\sigma_Y$ and $1.05\sigma_Y < \sigma_G < 1.24\sigma_Y$, where σ_Y is the yield stress. These observations, whilst not unique for high speed steels, contrast with the generally observed behaviour of metallic materials when $\sigma_N \geqslant \sigma_Y$ and subcritical crack growth is associated with a corrosive environment or dynamic loading.

4. In some ways the phenomenon of static subcritical crack growth in this metallic material resembles observations on ceramics, on which observations are now frequently reported as R-curve behaviour. When R-curves were plotted for this T1 high speed steel, the maximum value of the (estimated) microscopic stress intensity factor, K_a, approached the macroscopic K_{IC} for long cracks, independently determined; in contrast, e.g. to T42 where maximum K_a was as low as 0.5 K_{IC}.

Acknowledgements

The authors acknowledge the assistance of Dr M. Youseffi and the provision of a sectoral grant to one of us, MAG, by the European Union. The EU also financed the BRITE-EURAM project, contract No. R11B-104, in the course of which the sintered plus forged material was processed by SMK, Germany, in association with the University of Bradford.

References

1. A. S. WRONSKI, M. GOMES and C. S. WRIGHT, "Failure Analysis: Techniques and Applications", edited by J. I. Dickson, E. Abromovici and N. S. Marchand (ASM International, Materials Park, Ohio, USA, 1992) p. 1.
2. M. A. GOMES, A. S. WRONSKI and C. S. WRIGHT, *Fatigue Fract. Eng. Mater. Struct.* **18** (1995) 1.
3. M. A. GOMES, PhD thesis, University of Bradford (1993).
4. H. HUBNER and W. JILLEK, *J. Mater. Sci.* **12** (1977) 117.
5. Y.-W. MAI and B. LAWN, *J. Amer. Ceram. Soc.* **70** (1987) 289.
6. A. G. EVANS and K. T. FABER, *ibid.* **67** (1984) 255.
7. R. F. COOK and D. R. CLARKE, *Acta Metall.* **36** (1988) 555.
8. B. S. MAJUMDAR, A. R. ROSENFIELD and W. H. DUCKWORTH, *Eng. Fract. Mech.* **31** (1988) 683.
9. S. B. BINER, *Acta Metall. Mater.* **42** (1994) 3643.
10. C. S. WRIGHT, A. R. NUTTON and D. L. JONES, in P.M. '90–Proceedings of the World Conference on Powder Metallurgy, London, 1990, Vol. 3 (The Institute of Metals, London, 1990) p. 20.
11. W. J. C. PRICE, M. M. REBBECK, A. S. WRONSKI and S. A. AMEN, *Powder Met.* **28** (1985) 1.
12. K. ERIKSSON, *Scand. J. Metall.* **4** (1975) 182.
13. A. S. WRONSKI, L. B. H. AL-YASIRI and F. L. JAGGER, *Powder Met.* **22** (1979) 109.
14. C. S. WRIGHT, A. S. WRONSKI and M. M. REBBECK, *Metals Technol.* **11** (1984) 181.
15. J. D. BOLTON and M. YOUSEFFI, *Powder Met.* **36** (1993) 142.
16. A. S. WRONSKI, M. M. REBBECK and S. A. AMEN, *J. Mater. Sci.* **23** (1988) 2213.
17. G. BERRY and M. J. K. AL-TORNACHI, *Met. Technol.* **4** (1977) 289.
18. P. W. SHELTON and A. S. WRONSKI, "Towards Improved Performance of Tool Materials" edited by R. Irani (The Metals Society, London, 1981) p. 176.
19. J. A. RESCALVO and B. L. AVERBACH, *Met. Trans.* **10A** (1979) 1265.

20. F. A. BUTTERFIELD III and T. R. McNELLEY, *J. Tribology-Trans. ASME* **39** (1985) 1.
21. R. S. IRANI, C. S. WRIGHT and A. S. WRONSKI, *J. Mater. Sci. Lett.* **1** (1982) 318.
22. S. KARAGÖZ and H-O. ANDRÉN, *Z. Metallkd.* **83** (1992) 386.
23. P. BILLGREN and O. SANDBERG, in PM '94–Powder Metallurgy World Congress, Paris, 1994, Vol. II (Société Française de Métallurgie et de Matériaux, Paris, 1994) p. 1023.
24. A. NORDGREN, H. CHANDRASEKARAN and H. WISELL, in PM '94–Powder Metallurgy World Congress, Paris, 1994, Vol. II (Société Française de Métallurgie et de Matériaux, Paris, 1994) p. 1027.
25. S. A. HORTON and H. C. CHILD, *Metals Technol.* **10** (1983) 245.
26. M. H. POECH, H. F. FISCHMEISTER and K. HUMMERT, Proceedings of the First International High Speed Steel Conference, Leoben, 1990, edited by G. Hackl and B. Hribernik (Klampfer GmBH, Weiz, 1991) p. 73.
27. G. R. IRWIN, *J. Appl. Mech.* (*Trans. ASME*) **29** (1962) 651.
28. K. J. MILLER, *Mater. Sci. Technol.* **9** (1993) 453.

Received 6 February
and accepted 23 October 1996